NeuroImage: Clinical 12 (2016) 180–189

Contents lists available at ScienceDirect

NeuroImage: Clinical

journal homepage: www.elsevier.com/locate/ynicl

Hyperpolarized ^{13}C MR imaging detects no lactate production in mutant IDH1 gliomas: Implications for diagnosis and response monitoring

Myriam M. Chaumeil[a], Marina Radoul[a], Chloé Najac[a], Pia Eriksson[a], Pavithra Viswanath[a], Michael D. Blough[b], Charles Chesnelong[b], H. Artee Luchman[b], J. Gregory Cairncross[b], Sabrina M. Ronen[a,c,*]

[a]Department of Radiology and Biomedical Imaging, Mission Bay Campus, 1700 4th Street, Byers Hall, University of California, 94158 San Francisco, CA, United States
[b]Department of Clinical Neurosciences, Foothills Hospital, 1403 29 St NW, Calgary, AB T2N 2T9, Canada
[c]Brain Tumor Research Center, Helen Diller Family Cancer Research Building, 1450 3rd Street, University of California, 94158 San Francisco, CA, United States

ARTICLE INFO

Article history:
Received 26 May 2016
Received in revised form 21 June 2016
Accepted 22 June 2016
Available online 23 June 2016

Keywords:
Glioma
Isocitrate dehydrogenase 1 (IDH1) mutation
Metabolic reprogramming
Hyperpolarized ^{13}C Magnetic Resonance Spectroscopy (MRS)

ABSTRACT

Metabolic imaging of brain tumors using ^{13}C Magnetic Resonance Spectroscopy (MRS) of hyperpolarized [1-^{13}C] pyruvate is a promising neuroimaging strategy which, after a decade of preclinical success in glioblastoma (GBM) models, is now entering clinical trials in multiple centers. Typically, the presence of GBM has been associated with elevated hyperpolarized [1-^{13}C] lactate produced from [1-^{13}C] pyruvate, and response to therapy has been associated with a drop in hyperpolarized [1-^{13}C] lactate. However, to date, lower grade gliomas had not been investigated using this approach. The most prevalent mutation in lower grade gliomas is the isocitrate dehydrogenase 1 (IDH1) mutation, which, in addition to initiating tumor development, also induces metabolic reprogramming. In particular, mutant IDH1 gliomas are associated with low levels of lactate dehydrogenase A (LDHA) and monocarboxylate transporters 1 and 4 (MCT1, MCT4), three proteins involved in pyruvate metabolism to lactate. We therefore investigated the potential of ^{13}C MRS of hyperpolarized [1-^{13}C] pyruvate for detection of mutant IDH1 gliomas and for monitoring of their therapeutic response. We studied patient-derived mutant IDH1 glioma cells that underexpress LDHA, MCT1 and MCT4, and wild-type IDH1 GBM cells that express high levels of these proteins. Mutant IDH1 cells and tumors produced significantly less hyperpolarized [1-^{13}C] lactate compared to GBM, consistent with their metabolic reprogramming. Furthermore, hyperpolarized [1-^{13}C] lactate production was not affected by chemotherapeutic treatment with temozolomide (TMZ) in mutant IDH1 tumors, in contrast to previous reports in GBM. Our results demonstrate the unusual metabolic imaging profile of mutant IDH1 gliomas, which, when combined with other clinically available imaging methods, could be used to detect the presence of the IDH1 mutation *in vivo*.

1. Introduction

Magnetic resonance imaging (MRI), including sequences such as T2-weighted, T1-weighted post injection of Gadolinium contrast agent, or fluid attenuated inversion recovery (FLAIR), is the most widely used imaging modality in clinical neuro-oncology (Ryken et al., 2014). By providing anatomic and structural information about neoplasms and surrounding parenchyma, clinically-available MRI sequences enable diagnosis and grading of gliomas. However, complete assessment of brain tumor patients, including monitoring of

Abbreviations: 2-HG, 2-hydroxyglutarate; α-KG, α-ketoglutarate; AIF, arterial input function; AUC, area under the curve; DNP, dynamic nuclear polarization; DNP-MR, dynamic nuclear polarization magnetic resonance; EGF, epidermal growth factor; *EGFR*, epidermal growth factor receptor; FA, flip angle; FGF, fibroblast growth factor; FOV, field of view; FLAIR, fluid attenuated inversion recovery; GBM, glioblastoma; IDH1, isocitrate dehydrogenase 1; LDHA, lactate dehydrogenase A; MCT1, monocarboxylate transporter 1; MCT4, monocarboxylate transporter 4; MR, magnetic resonance; MRI, magnetic resonance imaging; MRS, magnetic resonance spectroscopy; MRS, magnetic resonance spectroscopic imaging; mTOR, mammalian target of rapamycin; NA, number of averages; NT, number of transients; PBS, phosphate-buffer saline; PDGF, platelet-derived growth factor; PET, positron emission tomography; PI3K, phosphoinositide 3-kinase; *PTEN*, phosphatase and tensin homolog; *RB1*, retinoblastoma protein 1; *SLC16A1*, solute carrier family 16 member 1; *SLC16A3*, solute carrier family 16 member 3; *SNR*, signal-to-noise ratio; SW, spectral width; Tacq, acquisition time; TCGA, The Cancer Genome Atlas; TE, echo time; TMZ, temozolomide; *TP53*, tumor protein p53; TR, repetition time; VOI, voxel of interest.

* Corresponding author at: 1700 4th Street, Box 2532, Byers Hall 3rd Floor, Suite 303, University of California, San Francisco 94143, CA, United States.
E-mail addresses: myriam.chaumeil@ucsf.edu (M.M. Chaumeil), marina.radoul@ucsf.edu (M. Radoul), chloe.najac@ucsf.edu (C. Najac), pia.eriksson@ucsf.edu (P. Eriksson), pavithra.viswanath@ucsf.edu (P. Viswanath), michaeldblough@gmail.com (M.D. Blough), cchesnel@ucalgary.ca (C. Chesnelong), aluchman@ucalgary.ca (H.A. Luchman), jgcairnx@ucalgary.ca (J.G. Cairncross), sabrina.ronen@ucsf.edu (S.M. Ronen).

http://dx.doi.org/10.1016/j.nicl.2016.06.018

early response to therapy and prediction of outcome, remain challenging (McKnight, 2004).

In an effort to address some of these challenges, multiple metabolic imaging stragegies have been developed (Chaumeil et al., 2015a; Chronaiou et al., 2014; Golman et al., 2006; Nelson et al., 2013b). In particular, ^{1}H MR spectroscopy (MRS), which can non-invasively assess steady-state metabolite levels, has been successfully used in the clinical setting to complement the anatomic and structural information generated by MRI, improving clinical practice (McKnight, 2004; Nelson, 2003). Over the past decade, an additional technique named ^{13}C MRS/spectroscopic imaging (MRSI) of hyperpolarized compounds has also shown great promise in preclinical studies (for reviews see references (Brindle et al., 2011; Chaumeil et al., 2015b; Kurhanewicz et al., 2011)). This imaging strategy, based on the dissolution dynamic nuclear polarization (DNP) method (Ardenkjaer-Larsen et al., 2003), increases the MR detectable signal-to-noise ratio (*SNR*) of hyperpolarized ^{13}C-labeled probes by over 10,000 fold, enabling direct monitoring of their metabolism in real time by ^{13}C MRS and MRSI. The conversion of hyperpolarized [1-^{13}C] pyruvate to [1-^{13}C] lactate catalyzed by the enzyme lactate dehydrogenase A (LDHA) has been the most commonly investigated reaction in oncology (Brindle et al., 2011; Chaumeil et al., 2015b; Kurhanewicz et al., 2011), as expression of LDHA is dramatically increased in most cancer types, associated with the "Warburg effect" (Warburg, 1956). In neuro-oncology, increased hyperpolarized [1-^{13}C] lactate production linked to overexpression of LDHA has been used for tumor detection in several preclinical murine models of glioblastoma (GBM) (Chaumeil et al., 2012; Park et al., 2011b; Park et al., 2010; Park et al., 2014; Venkatesh et al., 2012b; Ward et al., 2010a). Furthermore, this method was also shown to enable early imaging of response to targeted therapies and chemotherapy in GBM. A decrease in the hyperpolarized lactate-to-pyruvate ratio was observed in GBM cells following treatment with inhibitors of the phosphoinositide 3-kinase/mammalian target of rapamycin (PI3K/mTOR) pathway. It was correlated with a drop in LDHA activity, mRNA, and protein levels (Venkatesh et al., 2012b; Ward et al., 2010a) and this finding was further confirmed *in vivo* in orthotopic GBM tumors in rats (Chaumeil et al., 2012). Temozolomide (TMZ), the standard of care chemotherapeutic agent for GBM, was also shown to induce an early decrease in the hyperpolarized lactate-to-pyruvate ratio in orthotopic GBM models, alone (Park et al., 2011b; Park et al., 2014) or in combination with PI3K pathway inhibitors (Radoul et al., 2016). Importantly, the first in-man Phase I clinical trial of the technology was performed in 2013, and demonstrated that ^{13}C MRSI of hyperpolarized [1-^{13}C] pyruvate could be successfully used for tumor detection in prostate cancer patients (Nelson et al., 2013b). Several other trials, including ones for brain tumor patients, are now underway in many sites across the world (clinicaltrials.gov).

Despite the increased interest in translating the DNP-MR strategy to the clinical neuro-oncological setting, no preclinical studies have assessed the value of ^{13}C MRS of hyperpolarized [1-^{13}C] pyruvate in lower grade gliomas, which we now understand differ both genetically and metabolically from primary GBM (Goodenberger and Jenkins, 2012; Huse et al., 2011). Primary Grade IV GBM are associated with multiple genetic alterations including *EGFR* amplification and *TP53*, *PTEN*, and *RB1* mutation/loss (Cancer Genome Atlas Research, 2008). From a metabolic perspective, GBM tumors overexpress the LDHA enzyme, which catalyzes the pyruvate to lactate conversion (Cancer Genome Atlas Research, 2008), and increase the expression of the monocarboxylate transporters 1 and 4 (MCT1 and MCT4), which control cellular influx of pyruvate and efflux of lactate (Enerson and Drewes, 2003; Halestrap, 2012; Izumi et al., 2003; Parks et al., 2013; Pinheiro et al., 2012). In contrast, in lower grade Grade II and III oligodendroglioma and astrocytoma, as well as in secondary upgraded GBM, up to 90% of tumors harbor a mutation in the isocitrate dehydrogenase 1 (IDH1) enzyme (Cancer Genome Atlas Research N et al., 2015; Parsons et al., 2008; Yan et al., 2009). Mutant IDH1 catalyzes the reduction of α-ketoglutarate (α-KG) to 2-hydroxyglutarate (2-HG), resulting in non-physiological levels of this oncometabolite that induces epigenetic perturbations and ultimately leads to tumorigenesis (Dang et al., 2009; Yang et al., 2012). Importantly, the IDH1 mutation also leads to a broad and unusual reprogramming of cellular metabolism (Chesnelong et al., 2014; Elkhaled et al., 2014; Esmaeili et al., 2014; Grassian et al., 2014; Izquierdo-Garcia et al., 2014; Izquierdo-Garcia et al., 2015b; Ohka et al., 2014; Reitman et al., 2014; Reitman et al., 2011; Tonjes et al., 2013). By investigating clinically derived samples and cell models, we demonstrated that the genes coding for LDHA (*LDHA*), MCT4 (*SLC16A3*) and MCT1 (*SLC16A1*), that are typically overexpressed in GBM, are silenced or underexpressed in IDH1 mutant gliomas (Chesnelong et al., 2014; Luchman et al., 2012; Viswanath et al., 2016), suggesting an atypical pyruvate metabolism in these tumors.

We therefore decided to investigate the value of ^{13}C MRS of hyperpolarized [1-^{13}C] pyruvate for tumor detection and monitoring of therapeutic response in this tumor type. To do so, we investigated a recently developed patient-derived model of Grade III mutant IDH1 oligoastrocytoma, in which LDHA, MCT4 and MCT1 were shown to be underexpressed (Chesnelong et al., 2014; Viswanath et al., 2016). We also studied a previously established GBM cell line in which LDHA, MCT4 and MCT1 are readily detectable. Our metabolic imaging results show that hyperpolarized [1-^{13}C] lactate levels were barely detectable in mutant IDH1 glioma neurospheres and tumors, in contrast to the high levels detected in GBM. Furthermore, we found that TMZ treatment did not induce any significant changes in hyperpolarized [1-^{13}C] lactate levels in mutant IDH1 tumors, even though this therapeutic approach led to significant tumor shrinkage and increased survival. Considering the increasing translation of ^{13}C MRS of hyperpolarized [1-^{13}C] pyruvate to the clinic, our findings are highly significant for the proper interpretation of DNP-MR imaging data from brain tumor patients and point to an unexpected metabolic imaging signature of mutant IDH1 tumors. ^{13}C MRS of hyperpolarized [1-^{13}C] pyruvate must thus be used strategically to interrogate tumor type alongside other imaging modalities.

2. Material & methods

2.1. Cell models and culture

BT142 cells (Grade III oligoastrocytoma) were cultured as neurospheres in serum free NeuroCult NS-A Basal Medium (Stemcell technologies, Vancouver, BC) supplemented with 2 $\mu g \cdot mL^{-1}$ Heparin Solution (Stemcell technologies, Vancouver, BC), 20 $ng \cdot mL^{-1}$ EGF (Peprotech, Rocky Hill, NJ), 20 $ng \cdot mL^{-1}$ FGF (Peprotech, Rocky Hill, NJ), and 100 $ng \cdot mL^{-1}$ PDGF (BT142 only, Peprotech, Rocky Hill, NJ) (Chesnelong et al., 2014). U87 GBM cells were cultured as exponentially growing monolayers in high glucose Dulbecco's Modified Eagle Medium (DMEM H-21, UCSF Cell Culture Facility, San Francisco, CA) supplemented with 10% heat-inactivated fetal bovine serum (Thermo Scientific Hyclone, Logan, UT), 2 mM L-Glutamine, 100 $u \cdot mL^{-1}$ penicillin, and 100 $mg \cdot mL^{-1}$ streptomycin (UCSF Cell Culture Facility, San Francisco, CA). All cell lines were maintained at 37 °C in a humidified atmosphere of 95% air and 5% CO_2.

2.2. Perfusion system

For MRS studies of live cells, mutant IDH1 glioma cells ($n = 3$ BT142) were encapsulated in agarose beads and GBM cells ($n = 3$ U87) grown on microcarrier beads (NUNC) (Chesnelong et al., 2014; Venkatesh et al., 2012b; Ward et al., 2010a). After 24 h, ~3×10^7 cells were loaded into a 10-mm NMR tube and connected to a perfusion system (Chesnelong et al., 2014; Venkatesh et al., 2012b; Ward et al., 2010a). Briefly, an atmosphere of 5% CO_2/95% air was maintained in the perfusion system, and growth medium was circulated through the cells at a

flow rate of 1.5 mL·min^{-1} using a peristaltic pump. A port on the inflow line allowed for injection of the hyperpolarized pyruvate solution, during which time the perfusion was briefly stopped. Prior to and following each injection of hyperpolarized material, cell viability was confirmed by recording ^{31}P MR spectra. All experiments were performed at 37 °C.

2.3. Tumor bearing animals

The Institutional Animal Care and Use Committee of the University of California, San Francisco, approved all animal research. Athymic mice (BT142: Fox Chase SCID $n = 5$; U87: rnu/rnu homozygous $n = 5$; average weight 28 g; female; 6-week old at the time of intracranial injection; Charles River Laboratories, Wilmington, MA) were used. An hour before intracranial injection, BT142 or U87 cells were washed once with PBS, dissociated into single cells by trituration, counted and resuspended in NeuroCult NS-A Basal medium (BT142, Stemcell technologies, Vancouver, BC) or Dulbecco's Modified Eagle Medium (U87, DMEM H-21, UCSF Cell Culture Facility, San Francisco, CA) to a concentration of 1×10^5 cells per 3 μL. For intracranial injection, mice were anesthetized by intraperitoneal injection of ketamine/xylazine (100/20 mg·kg^{-1}). A volume of 3 μL of cell suspension was slowly injected into the right putamen using the freehand technique (Chaumeil et al., 2013; Chaumeil et al., 2012; Chesnelong et al., 2014). Buprenorphine (0.05 mg·kg^{-1}, V = 200 μL) and bupivacaine (5 mg·kg^{-1}, V = 50 μL) were injected subcutaneously before tumor cell injection and subsequent doses given at later time points according to veterinary recommendations in order to ensure optimal pain management.

For *in vivo* imaging studies, mice were anesthetized using isoflurane (1.5% in O_2, 1.5 L·min^{-1}) and a 27G catheter was secured in the tail-vein for injection of hyperpolarized material. During each MR session, temperature and respiration rates were continuously monitored and kept within a constant range to ensure animal well-being and to minimize the potential effect of isoflurane anesthesia on the metabolic measurements (Josan et al., 2013) (respiration: 80 ± 10 breaths per minute; temperature 37.0 ± 0.4 °C).

2.4. Temozolomide treatment

Once the tumor reached a size of ~100 mm^3 as assessed from T2-weighted MR images, BT142 tumor-bearing animals were treated with 4 ml.kg^{-1} TMZ ($n = 3$; Sigma Aldrich, St. Louis, MO) in Ora-Plus vehicle (Perrigo, Dublin, Ireland) by oral gavage at a dose of 5 mg·kg^{-1} (v = 150 μL per dose). TMZ was given once daily Monday to Friday for up to 70 days, after which time animals were euthanized.

2.5. Hyperpolarized [1-^{13}C] pyruvate

A volume of 6 μL (for cells) or 24 μL (for animals) of [1-^{13}C] pyruvate (14.1 M neat, 15 mM OX63 radical, 0.4 mM Dotarem) was polarized for ~1 h using a hypersense polarizer (Oxford Instruments) (Chaumeil et al., 2013; Chaumeil et al., 2012; Chesnelong et al., 2014; Park et al., 2014; Venkatesh et al., 2012a; Ward et al., 2010a). Hyperpolarized [1-^{13}C] pyruvate was then rapidly dissolved in isotonic buffer (40 mM Tris pH = 8, 3.0 μmol·L^{-1} Na_2EDTA for cell studies; 80 mM NaOH, 40 mM Tris pH = 8, 3.0 μmol·L^{-1} Na_2EDTA for animal studies). For cell studies, a volume of 3 mL of hyperpolarized [1-^{13}C] pyruvate was injected over 5 s to a final concentration of 5 mM. For animal studies, a volume of 300 μL of the 80 mM hyperpolarized [1-^{13}C] pyruvate solution was injected in the tail vein catheter over 12 s.

2.6. MR data acquisition in perfused cells

For cell studies, dynamic sets of hyperpolarized ^{13}C spectra were acquired on an 11.7 T INOVA high-resolution spectrometer (Agilent Technologies, Palo-Alto, CA) starting at the beginning of the pyruvate injection using a pulse-acquire sequence (13° flip angle (FA), 3 s repetition time (TR), total acquisition time Tacq = 300 s) (Chaumeil et al., 2013; Chesnelong et al., 2014; Ward et al., 2010a). ^{31}P MR spectra were acquired prior to and following ^{13}C MRS using a pulse-acquire sequence (proton-decoupled, 30° FA, TR = 3 s, spectral width SW = 10 kHz, 10,000 points, number of transients NT = 500) (Chesnelong et al., 2014; Venkatesh et al., 2012b; Ward et al., 2010a).

2.7. In vivo MR data acquisitions

All *in vivo* MR experiments were conducted on a mouse-dedicated 14.1 T MR system equipped with 100 G·cm^{-1} imaging gradients (Agilent Technologies, Palo-Alto, CA). For T2-weighted acquisitions, a single channel ^{1}H volume coil was used ($Ø_I = 40$ mm). ^{13}C metabolic imaging was performed using a dual tune ^{1}H-^{13}C volume coil ($Ø_I = 40$ mm).

BT142 tumor-bearing animals ($n = 5$ controls; $n = 3$ TMZ treated) and U87 tumor-bearing animals ($n = 5$ controls) were used in this study ($n = 13$ animals total). When the tumor reached ~100 mm^3, MR acquisitions were initiated. T2-weighted and ^{13}C MRSI post injection of hyperpolarized [1-^{13}C] pyruvate were conducted. T2-weighted imaging was performed to assess tumor size and location longitudinally using a 2D spin-echo multi-slice sequence with the following parameters: echo time TE/TR = 20/1200 ms; Field of View FOV = 30 × 30 mm^2; matrix 256 × 256; slice thickness 1 mm; 12 axial slices; number of averages NA = 2; Tacq = 10 min 14 sec.

For metabolic studies, 2D dynamic ^{13}C MRSI data were acquired at the start of the intravenous injection of hyperpolarized [1-^{13}C] pyruvate using the following parameters: TE/TR = 1.2/60 ms; SW = 2500 Hz; 128 points; 4 s temporal resolution; 3.4 mm in-plane resolution; FA 10 deg.; matrix 128 × 7 × 7; FOV 24 × 24 mm; 5 mm slice thickness; scan time 2.9 s per time points; 16 time points; Tacq = 48 s (Sukumar et al., 2012).

2.8. MR data analysis

Tumor size was measured from the T2-weighted MR images using the in-house SIVIC software, as previously described (Chaumeil et al., 2012; Nelson, 2001). Manual contouring of the tumor was performed in each axial slice, and the final volume was automatically calculated as the sum throughout slices of the tumor area times the slice thickness.

For spectroscopic data, all spectral assignments were based on literature reports (*e.g.* www.hmdb.ca). The integrals of hyperpolarized [1-^{13}C] pyruvate and hyperpolarized [1-^{13}C] lactate were quantified by peak integration of the dynamic hyperpolarized ^{13}C spectra using ACD/Spec Manager 9 (for cell studies) (Chesnelong et al., 2014; Venkatesh et al., 2012a; Ward et al., 2010a) or using the SIVIC software (for *in vivo* studies) (Chaumeil et al., 2013; Chaumeil et al., 2012; Chesnelong et al., 2014). For further quantification of cell and *in vivo* experiments, the area under the curve (AUC) of the dynamic signal of hyperpolarized [1-^{13}C] lactate and hyperpolarized [1-^{13}C] pyruvate were computed, and the ratio of the AUC of hyperpolarized [1-^{13}C] lactate to hyperpolarized [1-^{13}C] pyruvate (lactate/pyruvate) was calculated for each voxel of interest (VOI). For evaluation of substrate levels in each tumor type, hyperpolarized [1-^{13}C] pyruvate levels were calculated from the tumor VOI and from a VOI containing the major blood vessels in the animal neck. The ratio between the hyperpolarized [1-^{13}C] pyruvate levels (AUC) in those two regions was then calculated for each animal in order to compensate for variability in intravenous injections.

2.9. Western blotting analysis

One hour after the end of the last hyperpolarized ^{13}C MR experiment, untreated animals ($n = 5$ BT142, $n = 5$ U87) were euthanized. Brains were resected and rapidly dissected to isolate the tumor from the normal brain tissue. Tumors were then quickly snap-frozen in liquid N_2 and kept at −80 °C until further processing. Tumor tissues were later lysed using lysis buffer (Cell Signaling Technology) in the presence of

protease inhibitor (Calbiochem, Merck KGaA). For each cell line, ~1×10^6 cells were lysed using the same procedure.

For both cells and tumor lysates, Bradford analysis was first performed to assess protein content. Denatured proteins were then electrophoresed on 10% Biorad Ready gels (Life Science Research, Hercules, CA) using the SDS-PAGE method and electrotransferred onto polyvinylidene fluoride membranes ($n = 3$ for each cell line and each tumor type). Blots were probed for LDHA (dilution 1:100, Abcam, Cambridge, MA), MCT1 (dilution 1:400, Abcam, Cambridge, MA), MCT4 (dilution 1:400, Abcam, Cambridge, MA), and β-tubulin (dilution 1:1000, Cell Signaling Technology, Danvers, MA) and visualized using an enhanced chemiluminescence kit (ThermoFisher Scientific, Waltham, MA). Bands were quantified using the ImageJ software (NIH) and normalized to β-tubulin.

2.10. Statistical analysis

All results are expressed as mean ± standard deviation. For the survival study, survival probabilities were calculated according to the Kaplan–Meier method and compared with the log-rank test. For all other experiments, two-tailed Student *t*-test was used to determine the statistical significance of the results. A *p*-value below 0.05 was considered significant ($^*p < 0.05$; $^{**}p < 0.01$; $^{***}p < 0.005$).

3. Results

3.1. Unlike in GBM cells, hyperpolarized [1-^{13}C] lactate production is not elevated in mutant IDH1 glioma cells, associated with LDHA, MCT1 and MCT4 silencing

First we confirmed that our BT142 cells reduced expression of LDHA, MCT1 and MCT4, as previously reported by others (Chesnelong et al., 2014; Viswanath et al., 2016). Western blot analysis showed that LDHA and MCT4 were virtually silenced in BT142 cells, whereas both proteins were highly detectable in U87 cells (Fig. 1A; $LDHA^{BT142} = 1 \pm 1\%$ of U87; $MCT4^{BT142} = 1 \pm 1\%$ of U87; $n = 3$ for each cell line; $^{***}p < 0.005$). MCT1 expression was significantly lower in BT142 mutant IDH1 glioma cells as compared to U87 GBM cells, albeit to a lesser extent (Fig. 1A; $MCT1^{BT142} = 81 \pm 5\%$ of U87; $n = 3$ for each cell line; $^{**}p < 0.01$).

Following injection of hyperpolarized [1-^{13}C] pyruvate (δ = 172.9 ppm) into the medium of live U87 GBM cells and BT142 mutant IDH1 glioma neurospheres, production of hyperpolarized [1-^{13}C] lactate could be detected at 185 ppm. An example of ^{13}C spectral stack plot obtained in BT142 perfused cells is shown in Fig. 1B. However, when assessing the ratio of hyperpolarized [1-^{13}C] lactate to pyruvate AUC for each cell type, our analysis showed that the hyperpolarized lactate/pyruvate AUC ratio was significantly lower (97 ± 3%) in mutant IDH1 cells as compared to GBM cells, as shown in Fig. 1C & D. ($^{***}p < 0.005$).

3.2. Hyperpolarized [1-^{13}C] lactate production is not elevated in mutant IDH1 glioma tumors in vivo, in contrast to results in GBM tumors, and is associated with low LDHA and MCT4 expression

Next, we used ^{13}C MRSI of hyperpolarized [1-^{13}C] pyruvate *in vivo* to monitor orthotopic U87 and BT142 tumors in mice.

BT142 and U87 orthotopic tumors were readily detectable using T2-weighted MR imaging as illustrated in Fig. 2A. BT142 mutant IDH1 glioma tumors reached 100 mm^3 in 95 ± 12 days post intracranial injection whereas U87 GBM tumors reached the same size at 19 ± 6 days, consistent with the slower growth of lower grade mutant IDH1 tumors compared to GBM in patient data (Chung et al., 2015).

We then investigated hyperpolarized [1-^{13}C] lactate production from hyperpolarized [1-^{13}C] pyruvate. As shown in Fig. 2A & B, and in

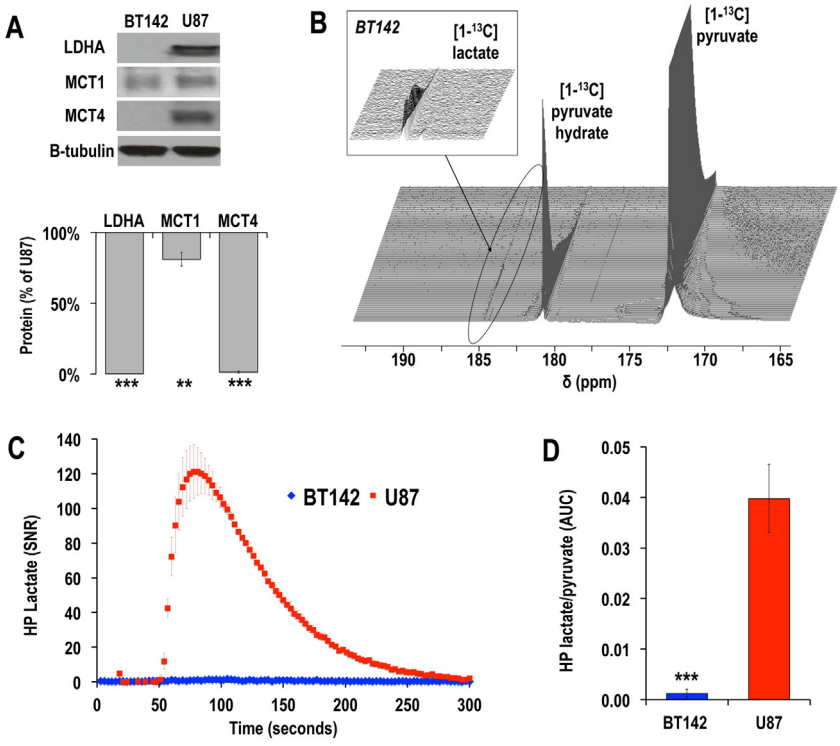

Fig. 1. Unlike in GBM cells, hyperpolarized [1-^{13}C] lactate production is not elevated in mutant IDH1 glioma cells, associated with LDHA, MCT1 and MCT4 silencing (A) Western blots for lactate dehydrogenase A (LDHA), monocarboxylate transporter 1 and 4 (MCT1, MCT4) for BT142 and U87 glioma cells and corresponding protein levels expressed as % of U87. (B) Stack plot of hyperpolarized ^{13}C MR spectra obtained at 11.7 T following injection of hyperpolarized [1-^{13}C] pyruvate (δ = 172.9 ppm) in the medium of perfused BT142 IDH1-mutant cells. Production of hyperpolarized [1-^{13}C] lactate could be detected at δ = 185 ppm (see insert). (C) Hyperpolarized [1-^{13}C] lactate signal-to-noise ratio (*SNR*) as a function of time for BT142 ($n = 3$) and U87 ($n = 3$) cells, showing the significantly lower level of lactate in mutant IDH1 gliomas as compared to glioblastoma. (D) Quantitative analysis of demonstrates that the hyperpolarized [1-^{13}C] lactate-to-pyruvate area-under-the-curve (AUC) was 97 ± 3% lower in BT142 compared to U87 cells ($n = 3$ for each cell line, $^{***}p < 0.005$).

line with previous studies in GBM tumors (Chaumeil et al., 2012; Park et al., 2011b; Park et al., 2010; Park et al., 2014; Venkatesh et al., 2012a; Ward and Thompson, 2012), high levels of hyperpolarized [1-^{13}C] lactate could be detected in U87 GBM tumors. In contrast, production of hyperpolarized [1-^{13}C] lactate in BT142 gliomas was barely above noise level. When comparing the two tumor types, our analysis showed a significantly lower (17 ± 7% of U87) level of hyperpolarized [1-^{13}C] lactate in BT142 tumors as compared to U87 GBM (Fig. 2C, hyperpolarized Lactate/Pyruvate$^{AUC}_{BT142}$ = 0.08 ± 0.03 *vs.* Lactate/Pyruvate$^{AUC}_{U87}$ = 0.48 ± 0.03; $^{*}p$ = 0.02), consistent with our results in perfused cells.

As shown in Fig. 2D, MCT1 levels were highly variable and not significantly different between U87 and BT142 tumors, (MCT1^{BT142} = 185 ± 104% of U87; $p > 0.05$). However, in line with our cell results, MCT4 and LDHA were virtually silenced in BT142 tumors, in contrast to high levels of expression detected in U87 GBM ($^{***}p < 0.005$; Fig. 2D & E).

3.3. Hyperpolarized [1-^{13}C] pyruvate levels are comparable between BT142 mutant IDH1 gliomas and U87 GBM tumors

Pyruvate transport into the cell is mediated primarily by MCT1 but also by MCT4 (Enerson and Drewes, 2003; Halestrap, 2012; Izumi et al., 2003; Parks et al., 2013; Pinheiro et al., 2012). We therefore wanted to rule out reduced hyperpolarized pyruvate delivery to the tumor as an explanation for the low levels of hyperpolarized lactate production observed in our mutant IDH1 tumor. To do so, we measured the levels of hyperpolarized pyruvate that reached the tumor VOI for both gliomas. As shown in Fig. 3, the level of hyperpolarized [1-^{13}C] pyruvate that reached the tumor VOI was not significantly different between U87 and BT142 animals (AUC Pyruvate$^{BT142}_{NdBlood}$ = 103 ± 35; AUC Pyruvate$^{U87}_{NdBlood}$ = 85 ± 21; p = 0.38). This result demonstrates a comparable substrate level *in situ*, and suggests that substrate availability did not play a major role in the observed difference in hyperpolarized [1-^{13}C] lactate production observed between BT142 and U87 tumors.

3.4. TMZ treatment leads to tumor shrinkage and improved survival, but does not induce a change in hyperpolarized [1-^{13}C] lactate production in mutant IDH1 glioma in vivo

Finally, we wanted to assess whether hyperpolarized [1-^{13}C] lactate production, which was previously shown to be altered by TMZ treatment in GBM, would be affected in any way by TMZ treatment in mutant IDH1 tumors. Our anatomic imaging showed that TMZ treatment induced a significant decrease in tumor size starting at day 14 of treatment, and ultimately led to a complete disappearance of the tumor on the T2-weighted MR images (after day 62, n = 3, Fig. 4A). Furthermore, TMZ treatment significantly increased the survival of BT142 tumor-bearing animals, as shown in Fig. 4B (χ^2 = 86.07; $^{***}p < 0.005$). However, in contrast to findings in GBM, our results show that the hyperpolarized [1-^{13}C] lactate-to-pyruvate ratio in the tumor voxel remained unchanged during the course of TMZ therapy (Fig. 4C & D, $p > 0.04$ for all time points).

4. Discussion

This study investigated the value of hyperpolarized ^{13}C MRS for detecting mutant IDH1 tumors and their response to treatment. We compared findings from the recently isolated, clinically-derived BT142 grade III mutant IDH1 model, to observations in a previously established primary Grade IV GBM model. Unlike pairs of genetically-engineered mutant and wild-type IDH1-expressing cells used in prior studies (Chaumeil et al., 2014; Chaumeil et al., 2013; Izquierdo-Garcia et al., 2014; Izquierdo-Garcia et al., 2015a; Izquierdo-Garcia et al., 2015b), this approach precludes a direct comparison between wild-type and mutant IDH1-associated events. However, it should be noted that an *in vivo* comparison between genetically engineered mutant and wild-type IDH1-expressing tumors is not straightforward. Most wild-type IDH1 cells that do not harbor additional genetic alterations (including the commonly used immortalized human astrocyte model (Izquierdo-Garcia et al., 2014;

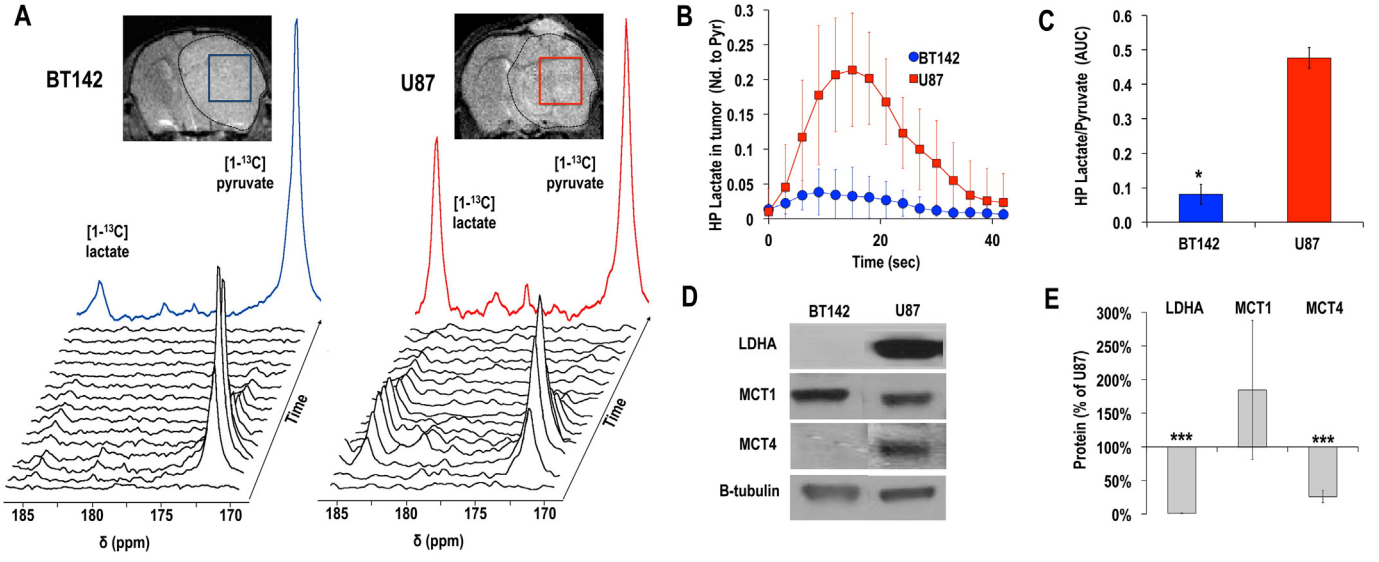

Fig. 2. Hyperpolarized [1-^{13}C] lactate production is not elevated in mutant IDH1 glioma tumors *in vivo*, in contrast to results in GBM tumors, and is associated with low LDHA and MCT4 expression (A) T2-weighted MR images of BT142 (left) and U87 (right) tumor bearing mice and positioning of tumor voxels (U87 red; BT142 blue). The tumor is circled in dashed lines. Corresponding stack plot of hyperpolarized ^{13}C MR spectra obtained at 14.1 Tesla following intravenous injection of hyperpolarized [1-^{13}C] pyruvate (δ = 172.9 ppm). Production of hyperpolarized [1-^{13}C] lactate could be detected in both tumor types at δ = 185 ppm, although the levels of hyperpolarized [1-^{13}C] lactate was lower in BT142 tumors as compared to U87. The color spectra represent the sum of the spectra over time (U87 red; BT142 blue). (B) Kinetics of hyperpolarized (HP) lactate normalized to maximum pyruvate in U87 (red, n = 5) and a BT142 (blue, n = 5) tumor voxels. (C) Analysis of the ratios of hyperpolarized [1-^{13}C] lactate-to-pyruvate AUC in tumor voxels demonstrates the significantly lower level of hyperpolarized [1-^{13}C] lactate production in BT142 tumors as compared to U87 ($^{*}p < 0.05$). (D) Western blots for lactate dehydrogenase A (LDHA), monocarboxylate transporters 1 and 4 (MCT1, MCT4) for BT142 and U87 tumor lysates and (E) corresponding protein levels expressed as % of U87 ($^{**}p < 0.01$; $^{***}p < 0.005$). (For interpretation of the references to color in this figure legend, the reader is referred to the web version of this article.)

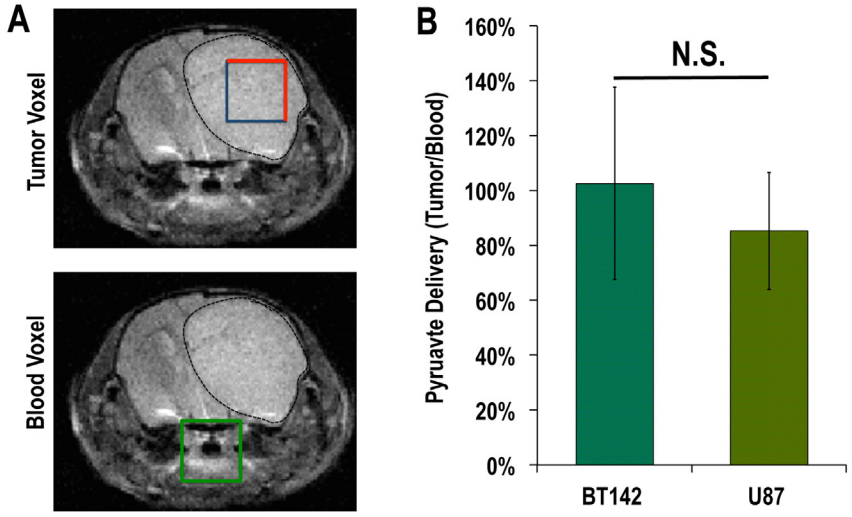

Fig. 3. *In vivo* hyperpolarized [1-^{13}C] pyruvate levels are comparable between tumor types (A) T2-weighted MR images showing the positioning of voxels of interest (VOI) from the tumor regions (blue/red) and from a region containing the major blood vessels in the animal neck (green). A BT142 tumor was chosen as an example in this figure. (B) Analysis of the ratios of pyruvate AUC in tumor VOI to the corresponding blood VOI demonstrated a comparable level of hyperpolarized [1-^{13}C] pyruvate in BT142 and U87 tumor voxels (N.S.: not significant). (For interpretation of the references to color in this figure legend, the reader is referred to the web version of this article.)

Izquierdo-Garcia et al., 2015a; Izquierdo-Garcia et al., 2015b; Sonoda et al., 2001)) fail to form tumors *in vivo*. As a result, previous *in vivo* comparisons have used models engineered from primary GBM, and therefore the metabolic findings could be confounded by events associated with GBM development. Furthermore, when investigating genetically engineered models, mutant IDH1-associated reprogramming depends on the

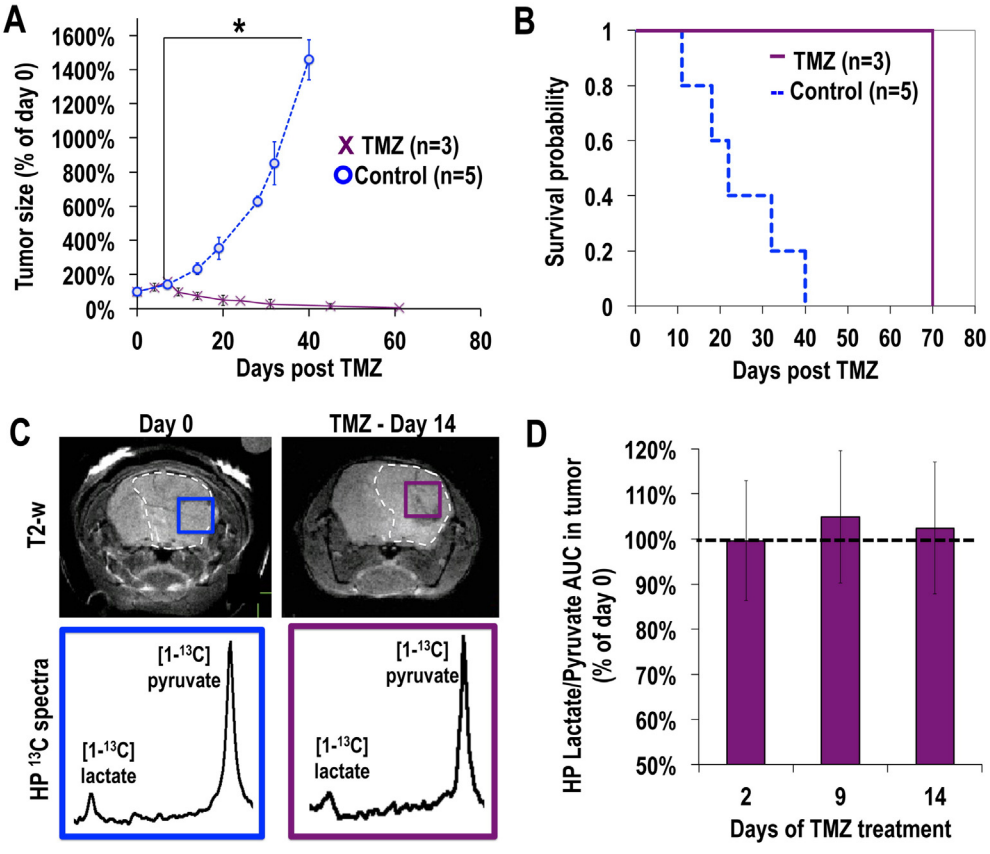

Fig. 4. Temozolomide (TMZ) treatment leads to tumor shrinkage and improved survival, but does not induce a change in hyperpolarized [1-^{13}C] lactate production in mutant IDH1 glioma *in vivo* (A) Evolution of tumor size in control (blue, $n = 5$) and TMZ-treated (purple, $n = 3$) animals as measured from T2-weighted MR imaging as a function of time post start of treatment, showing the significant tumor shrinkage in TMZ-treated animals as compared to controls. (B) Kaplan-Meier survival probability plot showing the increased survival of BT142 tumor-bearing animals induced by TMZ treatment ($\chi^2 = 86.07$; $^{***}p < 0.005$). (C) T2-weighted MR images of the brain of a BT142 tumor-bearing mouse at day 0 (blue, left) and day 14 (purple, right) post TMZ treatment overlaid with the grid used for hyperpolarized ^{13}C MR spectroscopic imaging. Corresponding ^{13}C spectra from tumor voxels show the comparable levels of hyperpolarized lactate and pyruvate pre and post treatment. (D) Analysis of the hyperpolarized [1-^{13}C] lactate-to-pyruvate AUC from tumor voxel normalized to day 0 ($n = 3$) demonstrates the unchanged level of lactate at days 2, 9 and 14 of TMZ treatment. (For interpretation of the references to color in this figure legend, the reader is referred to the web version of this article.)

number of passages that cells have been in culture (Turcan et al., 2012), also potentially limiting the significance of results. Here we investigated patient-derived models while linking our imaging findings to biological observations made in these and other models, as well as in The Cancer Genome Atlas (TCGA) clinical data (Chesnelong et al., 2014; Viswanath et al., 2016).

From a technical perspective, in our *in vivo* studies we used a novel 2D dynamic MRSI sequence allowing acquisition of the full hyperpolarized lactate and pyruvate kinetics. Unlike single time point sequences, which have been the most commonly used to date, this type of acquisition limits quantification errors due to temporal differences in the kinetics of substrate and products between different regions of interest, increasing the robustness of the acquired data (Sukumar et al., 2012). Furthermore, acquisition of dynamic data enabled us to conduct our analysis using the AUC ratio, which, as recently described by Daniels et al., performs significantly better than lactate-to-pyruvate ratio at the time of maximum lactate signal, and produces similar statistical results to any kinetic modeling Daniels et al. (2016)). Using this sequence and subsequent AUC analysis, we first demonstrated a high lactate-to-pyruvate AUC ratio in U87 tumors, in line with numerous previous studies on GBMs (Chaumeil et al., 2012; Park et al., 2011b; Park et al., 2010; Park et al., 2014; Radoul et al., 2015b). In contrast, in BT142 mutant IDH1 orthotopic tumors, hyperpolarized [1-^{13}C] lactate production was barely above noise level.

We also wanted to investigate if *in situ* substrate levels could be contributing to the detected differences in hyperpolarized [1-^{13}C] lactate production between tumor types. To do so, ideally one would want to measure the arterial input function (AIF) for each animal and each injection, similar to Positron Emission Tomography (PET) studies. However, measuring an AIF in DNP-MR studies remains challenging. It has only been evaluated in a few specialized studies *in vivo*, by using an implantable coil in the rat carotid (Marjańska et al., 2012), quantifying the signal from the injected hyperpolarized substrate in a catheter adjacent to the coil (Kazan et al., 2013), or by extrapolation of the data using a gamma-variate function (von Morze et al., 2011). Here, we used a more simplistic approach in which we compared the AUC of pyruvate in the tumor voxel to the same parameter in a voxel containing major neck blood vessels and no cerebral tissue. This approach, while not an AIF measurement, helps minimize confounding factors that affect the signal intensity in the tumor voxel, and in particular polarization level at the time of injection and inter-study variability in injection rates. Using this analysis, our results demonstrate a comparable level of hyperpolarized [1-^{13}C] pyruvate in BT142 and U87 tumor voxels, ruling out a major effect of substrate availability on the low hyperpolarized [1-^{13}C] lactate production observed in BT142 tumors.

Our biochemical results confirmed previous studies by Chesnelong et al. (Chesnelong et al., 2014) and Viswanath et al. (Viswanath et al., 2016) indicating LDHA and MCT4 silencing in mutant IDH1 BT142 gliomas, both in cell lysates and in resected tumor lysates. Additionally, we showed that MCT1 expression was lower in BT142 cell lysates than in U87 cell lysates, also in line with the report by Viswanath et al. (Viswanath et al., 2016). However, this observation did not hold in the *in vivo* setting. A possible reason for this is that MCT1 levels were only 19 ± 5% lower in BT142 cells than in U87 cells, as compared to >99% lower for LDHA and MCT4. It is thus likely that the difference in MCT1 levels between the two tumors was diluted by other cell types within the brain parenchyma, which typically presents high levels of MCT1 under physiological conditions (Chiry et al., 2006; Gerhart et al., 1997; Pierre et al., 2000).

LDHA, MCT1 and MCT4 are all involved in pyruvate metabolism, and their relative levels have been shown to play important roles in hyperpolarized [1-^{13}C] lactate production (Brindle et al., 2011; Chaumeil et al., 2015b; Kurhanewicz et al., 2011). The role of LDHA is most central, as this enzyme converts pyruvate into lactate. As such, *LDHA* silencing in mutant IDH1 tumors is entirely consistent with the low level of hyperpolarized [1-^{13}C] lactate detected in perfused cells and tumors in this study. When looking at the transporters, MCT4 primarily controls lactate efflux, whereas MCT1 mostly participates in pyruvate uptake (Enerson and Drewes, 2003; Halestrap, 2012; Izumi et al., 2003; Parks et al., 2013; Pinheiro et al., 2012). Interestingly, elevated expression of MCT4 has been linked to lower hyperpolarized [1-^{13}C] lactate production, through a decreased intracellular lactate pool (Keshari et al., 2013; Sriram et al., 2015). MCT4 silencing in BT142 cells and tumors is thus unlikely to contribute to the low hyperpolarized [1-^{13}C] lactate signal. On the other hand, we cannot rule out that the lower level of MCT1 in BT142 cells could contribute to the subsequent low production of hyperpolarized [1-^{13}C] lactate. However, in the *in vivo* setting, MCT1 levels were not significantly different between U87 and BT142 tumors, and hyperpolarized pyruvate levels were comparable, suggesting that the contribution of MCT1 to the differences in hyperpolarized [1-^{13}C] lactate levels between the tumor types is limited. It is important to note that, consistent with *LDHA* silencing, clinical studies have demonstrated that the steady-state levels of lactate observed by ^{1}H MRS are relatively low in low-grade glioma, the vast majority of which harbor the IDH1 mutation (Cancer Genome Atlas Research N, 2008; Parsons et al., 2008; Yan et al., 2009). Preclinical studies have also shown that intracellular lactate levels are lower in mutant IDH1 expressing cells compared to wild-type (Izquierdo-Garcia et al., 2015b). A small lactate pool size would, in turn, further contribute to the low level of hyperpolarized [1-^{13}C] lactate detected in BT142 tumors (Day et al., 2007). The contribution of intracellular lactate levels to the production of hyperpolarized lactate could be assessed in our models using dedicated sequences such as MAD-STEAM (Larson et al., 2012; Swisher et al., 2014) or diffusion-weighted DNP-MR (Koelsch et al., 2015). These would tease apart the respective contributions of the vascular, intracellular and extracellular compartments to the signal of each hyperpolarized metabolite. Nonetheless, regardless of the subtilities of the underlying mechanisms, our findings with regard to low hyperpolarized [1-^{13}C] lactate levels *in vivo* in BT142 tumors are likely primarily associated with *LDHA* silencing, and demonstrate the highly unusual imaging profile of this tumor type.

From a therapeutic perspective, a drop in hyperpolarized [1-^{13}C] lactate production has been consistently observed in response to treatment and is currently entering clinical trials as a biomarker of response in multiple cancer types including glioma (Chaumeil et al., 2015b; Chaumeil et al., 2012; Nelson et al., 2013a; Park et al., 2011a; Park et al., 2014; Radoul et al., 2015a; Venkatesh et al., 2012a; Ward et al., 2010b). We therefore wanted to clearly demonstrate that, unlike in other cancers, hyperpolarized [1-^{13}C] lactate is unlikely to be informative of response in mutant IDH1 gliomas. Our study showed that TMZ treatment induced a dramatic shrinkage of mutant IDH1 tumors that was associated with a significant increase in survival. This is in line with previous reports of high chemo-sensitivity for mutant IDH1 glioma (Cairncross et al., 2013), and points to the likely relevance of the BT142 model for assessment of therapeutic approaches for mutant IDH1 tumors. Furthermore, as expected, our findings with regard to using ^{13}C MRS of hyperpolarized [1-^{13}C] pyruvate for predicting response to therapy were in contrast to previous work in primary wild-type IDH1 GBM. Previous investigations of GBM models showed a significant decrease in hyperpolarized [1-^{13}C] lactate-to-pyruvate ratio as early as one day post treatment with TMZ and before any changes in tumor size (Park et al., 2011b; Park et al., 2014); our study in BT142 tumors shows that hyperpolarized lactate levels remained unchanged during TMZ treatment, even though tumor size decreased. This result not only demonstrates the unique metabolic profile of mutant IDH1 tumors following therapy, but also confirms the need for alternative imaging approaches for early assessment of drug action and for predicting response to TMZ in mutant IDH1 tumors.

5. Conclusion

Our results demonstrate that mutant IDH1 gliomas present a highly unusual metabolic imaging profile. Unlike any other cancer investigated to date, this tumor type is characterized by an absence of elevated hyperpolarized [1-^{13}C] lactate production. On one hand, this study highlights the limitation of ^{13}C MRS of hyperpolarized [1-^{13}C] pyruvate as a method for detection and monitoring of therapeutic response in mutant IDH1. On the other hand, the absence of elevated hyperpolarized [1-^{13}C] lactate can be viewed as a unique feature of mutant IDH1 gliomas. This imaging strategy could thus be combined with other metabolic imaging approaches such as ^{1}H MRS to detect elevated 2-HG levels (Andronesi et al., 2012; Choi et al., 2012; Elkhaled et al., 2012; Pope et al., 2012), or hyperpolarized ^{13}C MRS to monitor elevated [1-^{13}C] 2-HG (Chaumeil et al., 2013) and reduced [1-^{13}C] glutamate (Chaumeil et al., 2014) synthesis and, collectively, these imageable mutant IDH1-associated metabolic alterations that are detectable by MRS could serve to specifically identify mutant IDH1 tumors in patients.

Funding

This work was supported by the National Institute of Health (R01CA172845); Alberta Innovates Health Solutions; the Alberta Cancer Foundation and the UCSF Brain Tumor Center Loglio Collective.

Acknowledgment

The authors acknowledge support from the NIH-funded Hyperpolarized MRI Technology Resource Center (P41EB013598).

References

Andronesi, O.C., Kim, G.S., Gerstner, E., Batchelor, T., Tzika, A.A., Fantin, V.R., Vander Heiden, M.G., Sorensen, A.G., 2012. Detection of 2-hydroxyglutarate in IDH-mutated glioma patients by in vivo spectral-editing and 2D correlation magnetic resonance spectroscopy. Sci. Transl. Med. 4 (116), 116ra114.

Ardenkjaer-Larsen, J.H., Fridlund, B., Gram, A., Hansson, G., Hansson, L., Lerche, M.H., Servin, R., Thaning, M., Golman, K., 2003. Increase in signal-to-noise ratio of >10,000 times in liquid-state NMR. Proc. Natl. Acad. Sci. U. S. A. 100 (18), 10158–10163.

Brindle, K.M., Bohndiek, S.E., Gallagher, F.A., Kettunen, M.I., 2011. Tumor imaging using hyperpolarized 13C magnetic resonance spectroscopy. Magn. Reson. Med. 66 (2), 505–519.

Cairncross, G., Wang, M., Shaw, E., Jenkins, R., Brachman, D., Buckner, J., Fink, K., Souhami, L., Laperriere, N., Curran, W., Mehta, M., 2013. Phase III trial of chemoradiotherapy for anaplastic oligodendroglioma: long-term results of RTOG 9402. J. Clin. Oncol. Off. J. Am. Soc. Clin. Oncol. 31 (3), 337–343.

Cancer Genome Atlas Research N, 2008. Comprehensive genomic characterization defines human glioblastoma genes and core pathways. Nature 455 (7216), 1061–1068.

Cancer Genome Atlas Research N, Brat, D.J., Verhaak, R.G., Aldape, K.D., Yung, W.K., Salama, S.R., Cooper, L.A., Rheinbay, E., Miller, C.R., Vitucci, M., Morozova, O., Robertson, A.G., Noushmehr, H., Laird, P.W., Cherniack, A.D., Akbani, R., Huse, J.T., Ciriello, G., Poisson, L.M., Barnholtz-Sloan, J.S., Berger, M.S., Brennan, C., Colen, R.R., Colman, H., Flanders, A.E., Giannini, C., Grifford, M., Iavarone, A., Jain, R., Joseph, I., Kim, J., Kasaian, K., Mikkelsen, T., Murray, B.A., O'Neill, B.P., Pachter, L., Parsons, D.W., Sougnez, C., Sulman, E.P., Vandenberg, S.R., Van Meir, E.G., von Deimling, A., Zhang, H., Crain, D., Lau, K., Mallery, D., Morris, S., Paulauskis, J., Penny, R., Shelton, T., Sherman, M., Yena, P., Black, A., Bowen, J., Dicostanzo, K., Gastier-Foster, J., Leraas, K.M., Lichtenberg, T.M., Pierson, C.R., Ramirez, N.C., Taylor, C., Weaver, S., Wise, L., Zmuda, E., Davidsen, T., Demchok, J.A., Eley, G., Ferguson, M.L., Hutter, C.M., Mills Shaw, K.R., Ozenberger, B.A., Sheth, M., Sofia, H.J., Tarnuzzer, R., Wang, Z., Yang, L., Zenklusen, J.C., Ayala, B., Baboud, J., Chudamani, S., Jensen, M.A., Liu, J., Pihl, T., Raman, R., Wan, Y., Wu, Y., Ally, A., Auman, J.T., Balasundaram, M., Balu, S., Baylin, S.B., Beroukhim, R., Bootwalla, M.S., Bowlby, R., Bristow, C.A., Brooks, D., Butterfield, Y., Carlsen, R., Carter, S., Chin, L., Chu, A., Chuah, E., Cibulskis, K., Clarke, A., Coetzee, S.G., Dhalla, N., Fennell, T., Fisher, S., Gabriel, S., Getz, G., Gibbs, R., Guin, R., Hadjipanayis, A., Hayes, D.N., Hinoue, T., Hoadley, K., Holt, R.A., Hoyle, A.P., Jefferys, S.R., Jones, S., Jones, C.D., Kucherlapati, R., Lai, P.H., Lander, E., Lee, S., Lichtenstein, L., Ma, Y., Maglinte, D.T., Mahadeshwar, H.S., Marra, M.A., Mayo, M., Meng, S., Meyerson, M.L., Mieczkowski, P.A., Moore, R.A., Mose, L.E., Mungall, A.J., Pantazi, A., Parfenov, M., Park, P.J., Parker, J.S., Perou, C.M., Protopopov, A., Ren, X., Roach, J., Sabedot, T.S., Schein, J., Schumacher, S.E., Seidman, J.G., Seth, S., Shen, H., Simons, J.V., Sipahimalani, P., Soloway, M.G., Song, X., Sun, H., Tabak, B., Tam, A., Tan, D., Tang, J., Thiessen, N., Triche Jr., T., Van Den Berg, D.J., Veluvolu, U., Waring, S., Weisenberger, D.J., Wilkerson, M.D., Wong, T., Wu, J., Xi, L., Xu, A.W., Yang, L., Zack, T.I., Zhang, J., Aksoy, B.A., Arachchi, H., Benz, C., Bernard, B., Carlin, D., Cho, J., DiCara, D., Frazer, S., Fuller, G.N., Gao, J., Gehlenborg, N., Haussler, D., Heiman, D.I., Iype, L., Jacobsen, A., Ju, Z., Katzman, S., Kim, H., Knijnenburg, T., Kreisberg, R.B., Lawrence, M.S., Lee, W., Leinonen, K., Lin, P., Ling, S., Liu, W., Liu, Y., Liu, Y., Lu, Y., Mills, G., Ng, S., Noble, M.S., Paull, E., Rao, A., Reynolds, S., Saksena, G., Sanborn, Z., Sander, C., Schultz, N., Senbabaoglu, Y., Shen, R., Shmulevich, I., Sinha, R., Stuart, J., Sumer, S.O., Sun, Y., Tasman, N., Taylor, B.S., Voet, D., Weinhold, N., Weinstein, J.N., Yang, D., Yoshihara, K., Zheng, S., Zhang, W., Zou, L., Abel, T., Sadeghi, S., Cohen, M.L., Eschbacher, J., Hattab, E.M., Raghunathan, A., Schniederjan, M.J., Aziz, D., Barnett, G., Barrett, W., Bigner, D.D., Boice, L., Brewer, C., Calatozzolo, C., Campos, B., Carlotti Jr., C.G., Chan, T.A., Cuppini, L., Curley, E., Cuzzubbo, S., Devine, K., DiMeco, F., Duell, R., Elder, J.B., Fehrenbach, A., Finocchiaro, G., Friedman, W., Fulop, J., Gardner, J., Hermes, B., Herold-Mende, C., Jungk, C., Kendler, A., Lehman, N.L., Lipp, E., Liu, O., Mandt, R., McGraw, M., McLendon, R., McPherson, C., Neder, L., Nguyen, P., Noss, A., Nunziata, R., Ostrom, Q.T., Palmer, C., Perin, A., Pollo, B., Potapov, A., Potapova, O., Rathmell, W.K., Rotin, D., Scarpace, L., Schilero, C., Senecal, K., Shimmel, K., Shurkhay, V., Sifri, S., Singh, R., Sloan, A.E., Smolenski, K., Staugaitis, S.M., Steele, R., Thorne, L., Tirapelli, D.P., Unterberg, A., Vallurupalli, M., Wang, Y., Warnick, R., Williams, F., Wolinsky, Y., Bell, S., Rosenberg, M., Stewart, C., Huang, F., Grimsby, J.L., Radenbaugh, A.J., Zhang, J., 2015. Comprehensive, integrative genomic analysis of diffuse lower-grade gliomas. N. Engl. J. Med. 372 (26), 2481–2498.

Chaumeil, M.M., Ozawa, T., Park, I., Scott, K., James, C.D., Nelson, S.J., Ronen, S.M., 2012. Hyperpolarized 13C MR spectroscopic imaging can be used to monitor Everolimus treatment in vivo in an orthotopic rodent model of glioblastoma. NeuroImage 59 (1), 193–201.

Chaumeil, M.M., Larson, P.E., Yoshihara, H.A., Danforth, O.M., Vigneron, D.B., Nelson, S.J., Pieper, R.O., Phillips, J.J., Ronen, S.M., 2013. Non-invasive in vivo assessment of IDH1 mutational status in glioma. Nat. Commun. 4, 2429.

Chaumeil, M.M., Larson, P.E., Woods, S.M., Cai, L., Eriksson, P., Robinson, A.E., Lupo, J.M., Vigneron, D.B., Nelson, S.J., Pieper, R.O., Phillips, J.J., Ronen, S.M., 2014. Hyperpolarized [1-13C] glutamate: a metabolic imaging biomarker of IDH1 mutational status in glioma. Cancer Res. 74 (16), 4247–4257.

Chaumeil, M.M., Lupo, J.M., Ronen, S.M., 2015a. Magnetic resonance (MR) metabolic imaging in glioma. Brain Pathol. 25 (6), 769–780.

Chaumeil, M.M., Najac, C., Ronen, S.M., 2015b. Studies of metabolism using (13)C MRS of hyperpolarized probes. Methods Enzymol. 561, 1–71.

Chesnelong, C., Chaumeil, M.M., Blough, M.D., Al-Najjar, M., Stechishin, O.D., Chan, J.A., Pieper, R.O., Ronen, S.M., Weiss, S., Luchman, H.A., Cairncross, J.G., 2014. Lactate dehydrogenase a silencing in IDH mutant gliomas. Neuro-Oncology 16 (5), 686–695.

Chiry, O., Pellerin, L., Monnet-Tschudi, F., Fishbein, W.N., Merezhinskaya, N., Magistretti, P.J., Clarke, S., 2006. Expression of the monocarboxylate transporter MCT1 in the adult human brain cortex. Brain Res. 1070 (1), 65–70.

Choi, C., Ganji, S.K., Deberardinis, R.J., Hatanpaa, K.J., Rakheja, D., Kovacs, Z., Yang, X.L., Mashimo, T., Raisanen, J.M., Marin-Valencia, I., Pascual, J.M., Madden, C.J., Mickey, B.E., Malloy, C.R., Bachoo, R.M., Maher, E.A., 2012. 2-Hydroxyglutarate detection by magnetic resonance spectroscopy in IDH-mutated patients with gliomas. Nat. Med. 18 (4), 624–629.

Chronaiou, I., Stensjoen, A.L., Sjobakk, T.E., Esmaeili, M., Bathen, T.F., 2014. Impacts of MR spectroscopic imaging on glioma patient management. Acta Oncol. 53 (5), 580–589.

Chung, C., Metser, U., Menard, C., 2015. Advances in magnetic resonance imaging and positron emission tomography imaging for grading and molecular characterization of glioma. Semin. Radiat. Oncol. 25 (3), 164–171.

Dang, L., White, D.W., Gross, S., Bennett, B.D., Bittinger, M.A., Driggers, E.M., Fantin, V.R., Jang, H.G., Jin, S., Keenan, M.C., Marks, K.M., Prins, R.M., Ward, P.S., Yen, K.E., Liau, L.M., Rabinowitz, J.D., Cantley, L.C., Thompson, C.B., Vander Heiden, M.G., Su, S.M., 2009. Cancer-associated IDH1 mutations produce 2-hydroxyglutarate. Nature 462 (7274), 739–744.

Daniels, C., McLean, M.A., Schulte, R.F., Robb, F.J., Gill, A.B., McGlashan, N., Graves, M.J., Schwaiger, M., Lomas, D.J., Brindle, K., Gallagher, F.A., 2016. A comparison of quantitative methods for clinical imaging with hyperpolarized 13C-pyruvate. NMR Biomed. 29, 387–399.

Day, S.E., Kettunen, M.I., Gallagher, F.A., Hu, D.E., Lerche, M., Wolber, J., Golman, K., Ardenkjaer-Larsen, J.H., Brindle, K.M., 2007. Detecting tumor response to treatment using hyperpolarized 13C magnetic resonance imaging and spectroscopy. Nat. Med. 13 (11), 1382–1387.

Elkhaled, A., Jalbert, L.E., Phillips, J.J., Yoshihara, H.A., Parvataneni, R., Srinivasan, R., Bourne, G., Berger, M.S., Chang, S.M., Cha, S., Nelson, S.J., 2012. Magnetic resonance of 2-hydroxyglutarate in IDH1-mutated low-grade gliomas. Sci. Transl. Med. 4 (116), 116ra115.

Elkhaled, A., Jalbert, L., Constantin, A., Yoshihara, H.A., Phillips, J.J., Molinaro, A.M., Chang, S.M., Nelson, S.J., 2014. Characterization of metabolites in infiltrating gliomas using ex vivo (1)H high-resolution magic angle spinning spectroscopy. NMR Biomed. 27 (5), 578–593.

Enerson, B.E., Drewes, L.R., 2003. Molecular features, regulation, and function of monocarboxylate transporters: implications for drug delivery. J. Pharm. Sci. 92 (8), 1531–1544.

Esmaeili, M., Hamans, B.C., Navis, A.C., van Horssen, R., Bathen, T.F., Gribbestad, I.S., Leenders, W.P., Heerschap, A., 2014. IDH1 R132H mutation generates a distinct phospholipid metabolite profile in glioma. Cancer Res. 74 (17), 4898–4907.

Gerhart, D.Z., Enerson, B.E., Zhdankina, O.Y., Leino, R.L., Drewes, L.R., 1997. Expression of monocarboxylate transporter MCT1 by brain endothelium and glia in adult and suckling rats. Am. J. Phys. 273 (1 Pt 1), E207–E213.

Golman, K., Zandt, R.I., Lerche, M., Pehrson, R., Ardenkjaer-Larsen, J.H., 2006. Metabolic imaging by hyperpolarized 13C magnetic resonance imaging for in vivo tumor diagnosis. Cancer Res. 66 (22), 10855–10860.

Goodenberger, M.L., Jenkins, R.B., 2012. Genetics of adult glioma. Cancer Genet. 205 (12), 613–621.

Grassian, A.R., Parker, S.J., Davidson, S.M., Divakaruni, A.S., Green, C.R., Zhang, X., Slocum, K.L., Pu, M., Lin, F., Vickers, C., Joud-Caldwell, C., Chung, F., Yin, H., Handly, E.D., Straub, C., Growney, J.D., Vander Heiden, M.G., Murphy, A.N., Pagliarini, R., Metallo, C.M., 2014. IDH1 mutations alter citric acid cycle metabolism and increase dependence on oxidative mitochondrial metabolism. Cancer Res. 74 (12), 3317–3331.

Halestrap, A.P., 2012. The monocarboxylate transporter family—structure and functional characterization. IUBMB Life 64 (1), 1–9.

Huse, J.T., Phillips, H.S., Brennan, C.W., 2011. Molecular subclassification of diffuse gliomas: seeing order in the chaos. Glia 59 (8), 1190–1199.

Izquierdo-Garcia, J.L., Cai, L.M., Chaumeil, M.M., Eriksson, P., Robinson, A.E., Pieper, R.O., Phillips, J.J., Ronen, S.M., 2014. Glioma cells with the IDH1 mutation modulate metabolic fractional flux through pyruvate carboxylase. PloS One 9 (9), e108289.

Izquierdo-Garcia, J.L., Viswanath, P., Eriksson, P., Cai, L., Radoul, M., Chaumeil, M.M., Blough, M., Luchman, H.A., Weiss, S., Cairncross, J.G., Philips, J.J., Pieper, R.O., Ronen, S.M., 2015a. IDH1 mutation induces reprogramming of pyruvate metabolism. Cancer Res. 75 (15), 2999–3009.

Izquierdo-Garcia, J.L., Viswanath, P., Eriksson, P., Chaumeil, M.M., Pieper, R.O., Phillips, J.J., Ronen, S.M., 2015b. Metabolic reprogramming in mutant IDH1 glioma cells. PloS One 10 (2), e0118781.

Izumi, H., Torigoe, T., Ishiguchi, H., Uramoto, H., Yoshida, Y., Tanabe, M., Ise, T., Murakami, T., Yoshida, T., Nomoto, M., Kohno, K., 2003. Cellular pH regulators: potentially promising molecular targets for cancer chemotherapy. Cancer Treat. Rev. 29 (6), 541–549.

Josan, S., Hurd, R., Billingsley, K., Senadheera, L., Park, J.M., Yen, Y.F., Pfefferbaum, A., Spielman, D., Mayer, D., 2013. Effects of isoflurane anesthesia on hyperpolarized (13)C metabolic measurements in rat brain. Magn. Reson. Med. 70 (4), 1117–1124.

Kazan, S.M., Reynolds, S., Kennerley, A., Wholey, E., Bluff, J.E., Berwick, J., Cunningham, V.J., Paley, M.N., Tozer, G.M., 2013. Kinetic modeling of hyperpolarized (13)C pyruvate metabolism in tumors using a measured arterial input function. Magn. Reson. Med. 70 (4), 943–953.

Keshari, K.R., Sriram, R., Koelsch, B.L., Van Criekinge, M., Wilson, D.M., Kurhanewicz, J., Wang, Z.J., 2013. Hyperpolarized 13C-pyruvate magnetic resonance reveals rapid lactate export in metastatic renal cell carcinomas. Cancer Res. 73 (2), 529–538.

Koelsch, B.L., Reed, G.D., Keshari, K.R., Chaumeil, M.M., Bok, R., Ronen, S.M., Vigneron, D.B., Kurhanewicz, J., Larson, P.E., 2015. Rapid in vivo apparent diffusion coefficient mapping of hyperpolarized (13) C metabolites. Magn. Reson. Med. 74 (3), 622–633.

Kurhanewicz, J., Vigneron, D.B., Brindle, K., Chekmenev, E.Y., Comment, A., Cunningham, C.H., Deberardinis, R.J., Green, G.G., Leach, M.O., Rajan, S.S., Rizi, R.R., Ross, B.D., Warren, W.S., Malloy, C.R., 2011. Analysis of cancer metabolism by imaging hyperpolarized nuclei: prospects for translation to clinical research. Neoplasia 13 (2), 81–97.

Larson, P.E., Kerr, A.B., Swisher, C.L., Pauly, J.M., Vigneron, D.B., 2012. A rapid method for direct detection of metabolic conversion and magnetization exchange with application to hyperpolarized substrates. J. Magn. Reson. 225, 71–80.

Luchman, H.A., Stechishin, O.D., Dang, N.H., Blough, M.D., Chesnelong, C., Kelly, J.J., Nguyen, S.A., Chan, J.A., Weljie, A.M., Cairncross, J.G., Weiss, S., 2012. An in vivo patient-derived model of endogenous IDH1-mutant glioma. Neuro-Oncology 14 (2), 184–191.

Marjańska, M., Teisseyre, T.Z., Halpern-Manners, N.W., Zhang, Y., Iltis, I., Bajaj, V., Ugurbil, K., Pines, A., Henry, P.-G., 2012. Measurement of arterial input function in hyperpolarized 13C studies. Appl. Magn. Reson. 43 (1), 289–297.

McKnight, T.R., 2004. Proton magnetic resonance spectroscopic evaluation of brain tumor metabolism. Semin. Oncol. 31 (5), 605–617.

Nelson, S.J., 2001. Analysis of volume MRI and MR spectroscopic imaging data for the evaluation of patients with brain tumors. Magn. Reson. Med. 46 (2), 228–239.

Nelson, S.J., 2003. Multivoxel magnetic resonance spectroscopy of brain tumors. Mol. Cancer Ther. 2 (5), 497–507.

Nelson, S.J., Kurhanewicz, J., Vigneron, D.B., Larson, P.E.Z., Harzstarck, A., Ferrone, M., van Criekinge, M., Chang, J., Bok, R., Park, I., Reed, G., Carvajal, L., Small, E.J., Munster, P., Weinberg, V.K., Ardenkjaer-Larsen, J.H., Chen, A., Hurd, R., Odegardstuen, L., Robb, F.J., Tropp, J., Murray, J.A., 2013a. Metabolic imaging of patients with prostate cancer using hyperpolarized [1-13C]pyruvate. Sci. Transl. Med. (in press).

Nelson, S.J., Kurhanewicz, J., Vigneron, D.B., Larson, P.E., Harzstark, A.L., Ferrone, M., van Criekinge, M., Chang, J.W., Bok, R., Park, I., Reed, G., Carvajal, L., Small, E.J., Munster, P., Weinberg, V.K., Ardenkjaer-Larsen, J.H., Chen, A.P., Hurd, R.E., Odegardstuen, L.I., Robb, F.J., Tropp, J., Murray, J.A., 2013b. Metabolic imaging of patients with prostate cancer using hyperpolarized [1-(1)(3)C]pyruvate. Sci. Transl. Med. 5 (198), 198ra108.

Ohka, F., Ito, M., Ranjit, M., Senga, T., Motomura, A., Motomura, K., Saito, K., Kato, K., Kato, Y., Wakabayashi, T., Soga, T., Natsume, A., 2014. Quantitative metabolome analysis profiles activation of glutaminolysis in glioma with IDH1 mutation. Tumour Biol. 35 (6), 5911–5920.

Park, I., Larson, P.E., Zierhut, M.L., Hu, S., Bok, R., Ozawa, T., Kurhanewicz, J., Vigneron, D.B., Vandenberg, S.R., James, C.D., Nelson, S.J., 2010. Hyperpolarized 13C magnetic resonance metabolic imaging: application to brain tumors. Neuro-Oncology 12 (2), 133–144.

Park, I., Bok, R., Ozawa, T., Phillips, J.J., James, C.D., Vigneron, D.B., Ronen, S.M., Nelson, S.J., 2011a. Detection of early response to temozolomide treatment in brain tumors using hyperpolarized 13C MR metabolic imaging. J. Magn. Reson. Imaging 33 (6), 1284–1290.

Park, I., Bok, R., Ozawa, T., Phillips, J.J., James, C.D., Vigneron, D.B., Ronen, S.M., Nelson, S.J., 2011b. Detection of early response to temozolomide treatment in brain tumors using hyperpolarized 13C MR metabolic imaging. J. Magn. Reson. Imaging 33 (6), 1284–1290.

Park, I., Mukherjee, J., Ito, M., Chaumeil, M.M., Jalbert, L.E., Gaensler, K., Ronen, S.M., Nelson, S.J., Pieper, R.O., 2014. Changes in pyruvate metabolism detected by magnetic resonance imaging are linked to DNA damage and serve as a sensor of temozolomide response in glioblastoma cells. Cancer Res. 74 (23), 7115–7124.

Parks, S.K., Chiche, J., Pouyssegur, J., 2013. Disrupting proton dynamics and energy metabolism for cancer therapy. Nat. Rev. Cancer 13 (9), 611–623.

Parsons, D.W., Jones, S., Zhang, X., Lin, J.C., Leary, R.J., Angenendt, P., Mankoo, P., Carter, H., Siu, I.M., Gallia, G.L., Olivi, A., McLendon, R., Rasheed, B.A., Keir, S., Nikolskaya, T., Nikolsky, Y., Busam, D.A., Tekleab, H., Diaz Jr., L.A., Hartigan, J., Smith, D.R., Strausberg, R.L., Marie, S.K., Shinjo, S.M., Yan, H., Riggins, G.J., Bigner, D.D., Karchin, R., Papadopoulos, N., Parmigiani, G., Vogelstein, B., Velculescu, V.E., Kinzler, K.W., 2008. An integrated genomic analysis of human glioblastoma multiforme. Science (New York, N.Y.) 321 (5897), 1807–1812.

Pierre, K., Pellerin, L., Debernardi, R., Riederer, B.M., Magistretti, P.J., 2000. Cell-specific localization of monocarboxylate transporters, MCT1 and MCT2, in the adult mouse brain revealed by double immunohistochemical labeling and confocal microscopy. Neuroscience 100 (3), 617–627.

Pinheiro, C., Longatto-Filho, A., Azevedo-Silva, J., Casal, M., Schmitt, F.C., Baltazar, F., 2012. Role of monocarboxylate transporters in human cancers: state of the art. J. Bioenerg. Biomembr. 44 (1), 127–139.

Pope, W.B., Prins, R.M., Albert Thomas, M., Nagarajan, R., Yen, K.E., Bittinger, M.A., Salamon, N., Chou, A.P., Yong, W.H., Soto, H., Wilson, N., Driggers, E., Jang, H.G., Su, S.M., Schenkein, D.P., Lai, A., Cloughesy, T.F., Kornblum, H.I., Wu, H., Fantin, V.R., Liau, L.M., 2012. Non-invasive detection of 2-hydroxyglutarate and other metabolites in IDH1 mutant glioma patients using magnetic resonance spectroscopy. J. Neuro-Oncol. 107 (1), 197–205.

Radoul, M., Chaumeil, M.M., Eriksson, P., Ronen, S.M., 2015a. Hyperpolarized 13C MRSI is a Better Predictor of Survival Than Tumor Size in Treated Glioblastoma. International Society for Magnetic Resonance in Medicine, Toronto, ON.

Radoul, M., Chaumeil, M.M., Eriksson, P., Ronen, S.M., 2015b. Hyperpolarizied 13C MRSI is a Better Predictor of Survival Than Tumor Size in Treated Glioblastoma. ISMRM, Toronto, ON.

Radoul, M., Chaumeil, M.M., Eriksson, P., Wang, A.S., Phillips, J.J., Ronen, S.M., 2016. MR studies of glioblastoma models treated with dual PI3K/mTOR inhibitor and temozolomide — metabolic changes are associated with enhanced survival. Mol. Cancer Ther. 15 (5), 1113–1122.

Reitman, Z.J., Jin, G., Karoly, E.D., Spasojevic, I., Yang, J., Kinzler, K.W., He, Y., Bigner, D.D., Vogelstein, B., Yan, H., 2011. Profiling the effects of isocitrate dehydrogenase 1 and 2 mutations on the cellular metabolome. Proc. Natl. Acad. Sci. U. S. A. 108 (8), 3270–3275.

Reitman, Z.J., Duncan, C.G., Poteet, E., Winters, A., Yan, L.J., Gooden, D.M., Spasojevic, I., Boros, L.G., Yang, S.H., Yan, H., 2014. Cancer-associated isocitrate dehydrogenase 1 (IDH1) R132H mutation and d-2-hydroxyglutarate stimulate glutamine metabolism under hypoxia. J. Biol. Chem. 289 (34), 23318–23328.

Ryken, T.C., Aygun, N., Morris, J., Schweizer, M., Nair, R., Spracklen, C., Kalkanis, S.N., Olson, J.J., Committee, A.C.J.G., 2014. The role of imaging in the management of progressive glioblastoma: a systematic review and evidence-based clinical practice guideline. J. Neuro-Oncol. 118 (3), 435–460.

Sonoda, Y., Ozawa, T., Hirose, Y., Aldape, K.D., McMahon, M., Berger, M.S., Pieper, R.O., 2001. Formation of intracranial tumors by genetically modified human astrocytes defines four pathways critical in the development of human anaplastic astrocytoma. Cancer Res. 61 (13), 4956–4960.

Sriram, R., Van Criekinge, M., Hansen, A., Wang, Z.J., Vigneron, D.B., Wilson, D.M., Keshari, K.R., Kurhanewicz, J., 2015. Real-time measurement of hyperpolarized lactate production and efflux as a biomarker of tumor aggressiveness in an MR compatible 3D cell culture bioreactor. NMR Biomed. 28 (9), 1141–1149.

Sukumar, S., Hu, S., Larson, P.E., Zhang, V.Y., Ohliger, M., Bok, R., Kurhanewicz, J., Vigneron, D.B., 2012. Single-shot, 2D and 3D Dynamic Imaging of Hyperpolarized 13C Biomarkers In Vivo at 14.1 Tesla. ISMRM, Melbourne, Australia.

Swisher, C.L., Larson, P.E., Kruttwig, K., Kerr, A.B., Hu, S., Bok, R.A., Goga, A., Pauly, J.M., Nelson, S.J., Kurhanewicz, J., Vigneron, D.B., 2014. Quantitative measurement of cancer metabolism using stimulated echo hyperpolarized carbon-13 MRS. Magn. Reson. Med. 71 (1), 1–11.

Tonjes, M., Barbus, S., Park, Y.J., Wang, W., Schlotter, M., Lindroth, A.M., Pleier, S.V., Bai, A.H., Karra, D., Piro, R.M., Felsberg, J., Addington, A., Lemke, D., Weibrecht, I., Hovestadt, V., Rolli, C.G., Campos, B., Turcan, S., Sturm, D., Witt, H., Chan, T.A., Herold-Mende, C., Kemkemer, R., Konig, R., Schmidt, K., Hull, W.E., Pfister, S.M., Jugold, M., Hutson, S.M., Plass, C., Okun, J.G., Reifenberger, G., Lichter, P., Radlwimmer, B., 2013. BCAT1 promotes cell proliferation through amino acid catabolism in gliomas carrying wild-type IDH1. Nat. Med. 19 (7), 901–908.

Turcan, S., Rohle, D., Goenka, A., Walsh, L.A., Fang, F., Yilmaz, E., Campos, C., Fabius, A.W., Lu, C., Ward, P.S., Thompson, C.B., Kaufman, A., Guryanova, O., Levine, R., Heguy, A., Viale, A., Morris, L.G., Huse, J.T., Mellinghoff, I.K., Chan, T.A., 2012. IDH1 mutation is sufficient to establish the glioma hypermethylator phenotype. Nature 483 (7390), 479–483.

Venkatesh, H.S., Chaumeil, M.M., Ward, C.S., Haas-Kogan, D.A., James, C.D., Ronen, S.M., 2012a. Reduced phosphocholine and hyperpolarized lactate provide magnetic resonance biomarkers of PI3K/Akt/mTOR inhibition in glioblastoma. Neuro-Oncology 14 (3), 315–325.

Venkatesh, H.S., Chaumeil, M.M., Ward, C.S., Haas-Kogan, D.A., James, C.D., Ronen, S.M., 2012b. Reduced phosphocholine and hyperpolarized lactate provide magnetic resonance biomarkers of PI3K/Akt/mTOR inhibition in glioblastoma. Neuro-Oncology 14 (3), 315–325.

Viswanath, P., Najac, C., Izquierdo-Garcia, J.L., Pankov, A., Hong, C., Eriksson, P., Costello, J.F., Pieper, R.O., Ronen, S.M., 2016. Mutant IDH1 gliomas down-regulate expression of monocarboxylate transporters. Oncotarget. http://dx.doi.org/10.18632/oncotarget.9006 (in press).

von Morze, C., Larson, P.E., Hu, S., Keshari, K., Wilson, D.M., Ardenkjaer-Larsen, J.H., Goga, A., Bok, R., Kurhanewicz, J., Vigneron, D.B., 2011. Imaging of blood flow using hyperpolarized [(13)C]urea in preclinical cancer models. J. Magn. Reson. Imaging 33 (3), 692–697.

Warburg, O., 1956. On the origin of cancer cells. Science 123 (3191), 309–314.
Ward, P.S., Thompson, C.B., 2012. Metabolic reprogramming: a cancer hallmark even warburg did not anticipate. Cancer Cell 21 (3), 297–308.
Ward, C.S., Venkatesh, H.S., Chaumeil, M.M., Brandes, A.H., Vancriekinge, M., Dafni, H., Sukumar, S., Nelson, S.J., Vigneron, D.B., Kurhanewicz, J., James, C.D., Haas-Kogan, D.A., Ronen, S.M., 2010a. Noninvasive detection of target modulation following phosphatidylinositol 3-kinase inhibition using hyperpolarized 13C magnetic resonance spectroscopy. Cancer Res. 70 (4), 1296–1305.
Ward, C.S., Venkatesh, H.S., Chaumeil, M.M., Brandes, A.H., Vancriekinge, M., Dafni, H., Sukumar, S., Nelson, S.J., Vigneron, D.B., Kurhanewicz, J., James, C.D., Haas-Kogan, D.A., Ronen, S.M., 2010b. Noninvasive detection of target modulation following phosphatidylinositol 3-kinase inhibition using hyperpolarized 13C magnetic resonance spectroscopy. Cancer Res. 70 (4), 1296–1305.
Yan, H., Parsons, D.W., Jin, G., McLendon, R., Rasheed, B.A., Yuan, W., Kos, I., Batinic-Haberle, I., Jones, S., Riggins, G.J., Friedman, H., Friedman, A., Reardon, D., Herndon, J., Kinzler, K.W., Velculescu, V.E., Vogelstein, B., Bigner, D.D., 2009. IDH1 and IDH2 mutations in gliomas. N. Engl. J. Med. 360 (8), 765–773.
Yang, H., Ye, D., Guan, K.L., Xiong, Y., 2012. IDH1 and IDH2 mutations in tumorigenesis: mechanistic insights and clinical perspectives. Clin. Cancer Res. 18 (20), 5562–5571.